


Key Lipoprotein Receptor Targeted Echinacoside-Liposomes Effective Against Parkinson's Disease in Mice Model

Zemin Ou , Yun You, Hong Yi, Xiaoqian Liu, Yan Tong, Dewen Liu, Jinyu Wang 

Institute of Chinese Materia Medica, China Academy of Chinese Medical Sciences, Beijing, People's Republic of China

Correspondence: Dewen Liu; Jinyu Wang, Institute of Chinese Materia Medica, China Academy of Chinese Medical Sciences, Beijing, 10700, People's Republic of China, Email dwliu@icmm.ac.cn; wangjinyu@icmm.ac.cn

Introduction: Parkinson's disease (PD) is a common neurodegenerative disorder characterized by the degeneration of dopaminergic neurons in the substantia nigra. The precise molecular mechanisms underlying neuronal loss in PD remain unknown, and there are currently no effective treatments for PD-associated neurodegeneration. Echinacoside (ECH) is known for its neuroprotective effects, which include scavenging cellular reactive oxygen species and promoting mitochondrial fusion. However, the blood-brain barrier (BBB) limits the bioavailability of ECH in the brain, posing a significant challenge to its use in PD treatment.

Methods: We synthesized and characterized PEGylated ECH liposomes (ECH@Lip) and peptide angiopep-2 (ANG) modified liposomes (ECH@ANG-Lip). The density of ANG in ANG-Lip was optimized using bEnd.3 cells. The brain-targeting ability of the liposomes was assessed in vitro using a transwell BBB model and in vivo using an imaging system and LC-MS. We evaluated the enhanced neuroprotective properties of this formulation in a the 1-methyl-4-phenyl-1,2,3,6-tetrahydropyridine (MPTP)-induced PD model.

Results: The ECH@ANG-Lip demonstrated significantly higher whole-brain uptake compared to ECH@Lip and free ECH. Furthermore, ECH@ANG-Lip was more effective in mitigating MPTP-induced behavioral impairment, oxidative stress, dopamine depletion, and dopaminergic neuron death than both ECH@Lip and free ECH.

Conclusion: The formulation used in our study significantly enhanced the neuroprotective efficacy of ECH in the MPTP-induced PD model. Thus, ECH@ANG-Lip shows considerable potential for improving the bioavailability of ECH and providing neuroprotective effects in the brain.

Keywords: nanomedicine, brain delivery, angiopep-2, echinacoside, Parkinson's disease, liposomes

Introduction

Parkinson's disease (PD) is a progressive neurodegenerative disorder characterized by bradykinesia, rigidity, and tremor.¹⁻³ Although the complete pathogenesis of PD remains unclear, the disease's pathological manifestations and clinical symptoms are linked to the chronic degeneration of dopaminergic neurons in the substantia nigra, leading to decreased dopamine secretion in the striatum.⁴⁻⁶ Levodopa is the first-line treatment for PD, as it replenishes the dwindling supply of dopamine in the brain. However, prolonged use of levodopa at high doses can increase the risk of dyskinesia.⁷⁻⁹ Additionally, the conversion of levodopa to dopamine is facilitated by the decarboxylase enzyme, which exhibits reduced activity in the brains of PD patients.¹⁰ Currently, there are no effective therapeutic interventions that can inhibit dopaminergic neurodegeneration in the substantia nigra.

Echinacoside (ECH) is a naturally occurring phenylethanol glycoside with diverse pharmacological properties, including neuroprotection through scavenging cellular reactive oxygen species and promoting mitochondrial fusion via targeting casein kinase 2.^{11,12} Despite these beneficial effects, ECH's oral bioavailability is merely 0.83%, and its permeability across the blood-brain barrier (BBB) is limited. Consequently, ECH may not exert direct neuroprotective

effects on dopaminergic neurons.^{13,14} Implementing a drug delivery system to facilitate the transportation of ECH across the BBB and enable its direct interaction with dopaminergic neurons represents a novel therapeutic approach.

Various drug delivery systems have been developed to optimize the transportation of pharmacological agents across the BBB.^{15–17} Liposomes, composed of phospholipid bilayers, are effective nanocarriers for this purpose.^{18–20} To optimize brain delivery, the size of liposomes is carefully controlled to remain below 100 nm, and their surfaces can be modified with ligands that selectively bind to receptors on brain endothelial cells.²¹ Cationic liposomes, which engage in electrostatic interactions with anionic regions of the cellular membrane, can enhance BBB crossing.^{22,23} Additionally, modifying the liposome surface by incorporating ligands capable of binding to brain endothelial cell receptors can further improve BBB penetration.^{24,25}

Angiopep-2 (ANG) is a 2.4 kDa peptide with a strong affinity for the low-density lipoprotein receptor-related protein-1 (LRP1), which is overexpressed on brain endothelial cells.^{26–30} Due to its continuous endocytosis from the membrane and recycling, LRP1 becomes an attractive candidate for BBB targeting.³¹ These characteristics have been utilized in the context of targeted drug delivery across the BBB to the brain, specifically through receptor-mediated transcytosis.^{29,32} Studies have shown that ANG demonstrates a higher capacity for transcytosis via bovine brain endothelial cells compared to other ligands like lactoferrin, transferrin, and avidin.³³ Although ANG has been partially studied and applied as a brain-targeting ligand, few studies have investigated the impact of the number of ANG ligand molecules on the carrier surface on transmembrane transport efficiency.

In this study, we synthesized ANG-conjugated ECH-loaded liposomes (ECH@ANG-Lip) to assess their uptake by bEnd.3 cells and transport efficiency using an in vitro BBB model. The ECH@ANG-Lip formulation was designed to selectively interact with LRP1 receptors, which are highly expressed on the BBB. We hypothesized that liposomes loaded with ECH and targeted towards LRP1 would enhance brain targeting efficacy, resulting in higher ECH concentrations in the brain. Furthermore, we anticipated that this formulation would improve neuroprotective effects in a mouse model of PD induced by MPTP. The modification of liposome surfaces with ANG is expected to increase brain uptake, offering potential therapeutic benefits.

Materials and Methods

Soybean phosphatidylcholine (SPC) and cholesterol (Chol) were obtained through acquisition from AVT Pharmaceutical Tech Co., Ltd (Shanghai, China). Peptide ANG with C-terminal cysteine (TFFFYGGSRGKRNKTEEY-Cys), DSPE-PEG_{2K}-MAL, and DSPE-PEG_{2K} were bought from Guangzhou Carbohydrate Biotechnology Co., Ltd (Guangzhou, China). ECH and verbascoside were acquired from Chengdu Herbpurify Co., Ltd (Chengdu, China). MPTP, levodopa, dopamine hydrochloride, 3,4-dihydroxyphenylacetic acid, and homovanillic acid were from Shanghai Yuanze Biological Technology Co., Ltd (Shanghai, China). Rhodamine B (RhB) was acquired from Shanghai Aladdin Bio-Chem Technology Co., Ltd (Shanghai, China). 1,10-Dioctadecyl-3,3',3'',3'''-tetramethylindotricarbocyanine iodide (DiR) and DAPI were acquired from Beijing Biorigin Biotechnology Co., Ltd (Beijing, China). The Enhanced Cell Counting Kit-8 (CCK-8) was procured from Beyotime Biotechnology Co., Ltd (Shanghai, China). The DMEM used in this study contained high levels of glucose and was obtained from Gemini Bio-products (West Sacramento, CA). Additionally, fetal bovine serum (FBS) from the same source was also utilized. A trypsin solution with a concentration of 0.25% (w/v) was acquired from Gibco BRL (Grand Island, NY, USA). The acquisition of bEnd.3 cell lines was made from Procell Life Science & Technology Co., Ltd (Wuhan, China). The chemicals and reagents employed in this investigation were of analytical grade and were acquired from commercial sources.

The Synthesis of Key Liposomes Using the Thin-Film Hydration Approach

For the preparation of PEGylated ECH liposomes (ECH@Lip), SPC, Chol, DSPE-PEG_{2K}, and ECH (in a weight ratio of 30:6:6:5) were dissolved in a chloroform and methanol mixture (volume ratio of 2:1). The organic solvents were evaporated, leaving behind a thin film, which was then hydrated with a saline solution. This mixture was subjected to intermittent sonication using a probe sonicator operating at a power of 60 W for 8 minutes, resulting in the formation of ECH@Lip. The preparation of maleimide-derivatized PEGylated ECH liposomes (ECH@MAL-Lip) followed the same procedure as ECH@Lip but used SPC, Chol, DSPE-PEG_{2K}, DSPE-PEG_{2K}-MAL, and ECH in a weight ratio of

30:6:3:6:5. For peptide ANG-modified liposomes (ECH@ANG-Lip), a maleimide-thiol coupling reaction between DSPE-PEG_{2K}-MAL and ANG was performed at 4°C for 12 hours. Free ANG was removed using an ultrafiltration tube with a molecular weight cutoff of 3 kDa. The coupling efficiency of ANG was measured using UPLC (UPLC conditions are provided in the [supplementary materials](#)). To confirm the linkage between ANG and DSPE-PEG_{2K}-MAL, both ANG-conjugated and non-conjugated liposomes were dissolved in DMSO-d₆ and analyzed using an Ascend 600 NMR spectrometer (Bruker, Ettlingen, Germany).

Optimization of the Modified Density of Angiopep-2 in Liposomes

The efficiency of receptor recognition by target cells may be influenced by the density of ligands on the liposomes.³⁴ To investigate this, RhB@ANG-Lip formulations with varying densities of ANG (0%, 2%, 4%, 6%, and 8%) were synthesized by adjusting the molar ratio of DSPE-PEG_{2K}, DSPE-PEG_{2K}-MAL, and ANG. The RhB@ANG-Lip formulations were prepared using the thin-film hydration technique, incorporating SPC, Chol, DSPE-PEG_{2K}, DSPE-PEG_{2K}-MAL, ANG, and RhB. The cellular uptake of RhB@ANG-Lip with various ANG densities was examined in bEnd.3 cells using fluorescence microscopy and flow cytometry.

Particle Size and Zeta Potential

The particle size and zeta potential of the liposomes were determined at 25°C using dynamic light scattering with a Zetasizer Nano ZS nanoparticle sizer (Malvern Instruments, UK).

The Electron Microscopy

The morphological examinations of ECH@Lip and ECH@ANG-Lip were performed using transmission electron microscopy (TEM, JEM1200EX, Japan). Briefly, the liposomes were negatively stained with a 1% phosphotungstic acid solution and then immobilized on a 200-mesh copper grid.

The Encapsulation Efficiency and Loading Capacity

The encapsulation efficiency (EE) and loading capacity (LC) of the liposomes were determined using an ultrafiltration technique to separate free drugs from the liposomes. The liposomes were centrifuged at 15,294 g for 15 minutes to remove unencapsulated drugs. The amount of ECH in the supernatant was measured by UPLC (UPLC conditions are provided in the supplementary materials). The EE (%) and LC (%) values of ECH in the liposomes were calculated using the following formulas:

$$EE\% = \frac{W_{\text{total}} - W_{\text{free}}}{W_{\text{total}}} \times 100\%$$

$$LC\% = \frac{W_{\text{total}} - W_{\text{free}}}{W_{\text{total amount of liposomes}}} \times 100\%$$

where “W_{total}” is the weight of total ECH in liposomes and “W_{free}” is the mass of the free drug from the liposomes.

Stability Evaluation

Liposome placement stability: ECH@Lip and ECH@ANG-Lip were stored at 4°C after preparation. The particle size and encapsulation efficiency were measured on days 0, 1, 3, 5, and 7.

Stability of liposomes in serum: ECH@Lip and ECH@ANG-Lip were incubated with 10% FBS at 37°C. The particle size of the liposomes was measured at 0, 2, 4, 6, 12, 24, and 48 hours.

In vitro Drug Release Studies

In vitro, the release of ECH from liposomes was assessed in saline. Specifically, 1 mL of ECH@Lip and ECH@ANG-Lip solutions, each containing 1.5 mg of ECH, were placed in dialysis tubes with a MWCO of 3500 Da. The tubes were sealed and immersed in 15 mL of release medium, then incubated at 37°C with gentles shaking for 24 hours. After

incubation, 0.5 mL of the release medium was collected, and an equal volume of pre-warmed fresh release medium was added as a replacement. The concentrations of ECH were then determined using UPLC analysis.

In vitro Blood-Brain Barrier Penetration Capability

The in vitro BBB model was established following the methodology outlined in the referenced paper.³⁵ Briefly, bEnd.3 cells were cultured at a density of 1×10^5 cells/cm² in 12-well transwell inserts (Corning, Kennebunk ME, USA). After one week, the transwell membranes in the donor chambers formed uniform and compact monolayers. The transendothelial electric resistance (TEER) of the monolayers was measured using the Millicell ERS instrument (Millipore, Massachusetts, USA). The BBB models were considered successfully created when the TEER value exceeded 200 $\Omega \cdot \text{cm}^{-2}$. Subsequently, the apparent permeability coefficients of fluorescein sodium were assessed. Three cell monolayers were exposed to 0.5 mL of a fluorescein sodium solution with a concentration of 2 $\mu\text{g/mL}$, while the acceptor chambers received 1.5 mL of DMEM without phenol red. At specific time intervals (15, 30, 45, and 60 minutes), 100 μL aliquots were collected and analyzed for concentration using a SpectraMax i3 fluorescent microplate reader (Molecular Devices, Sunnyvale, CA, USA). The permeability coefficients (cm/s) were then calculated using the following equation:

$$P_{\text{apparent}} = \frac{\frac{dQ}{dt}}{C_0 * SA}$$

where the $\frac{dQ}{dt}$ is the rate of transfer of fluorescein sodium through the cell layer, C_0 is the initial concentration of the donor, and SA is the Transwell filter support's surface area.

Based on the previously validated in vitro BBB model, 0.5 mL of ECH@Lip, ECH@ANG-Lip, and ECH@ANG-Lip + ANG (with ECH at 1.5 mg/mL and ANG at 1 mg/mL) were introduced into the donor chambers. For the ECH@ANG-Lip + ANG cohort, the cells were pretreated with fresh ANG peptide for 1 hour prior to application. At regular intervals, 200 μL samples were collected and replaced with an equal volume of DMEM without phenol red. UPLC was employed to quantify the samples and determine the concentration of ECH, from which the permeability efficiency (Pe%) was calculated using the following equation:

$$P_e \% = \frac{C_t \times V_{\text{acceptor}}}{C_0 \times V_{\text{donor}}} \times 100\%$$

where C_t and C_0 are the ECH concentrations in the acceptor chamber at a given time and the original ECH concentration in the donor chamber, respectively. V_{acceptor} and V_{donor} are 1.5 mL and 0.5 mL, respectively.

Hemolysis Test

A hemolysis assay was performed to evaluate the biocompatibility of ECH@Lip and ECH@ANG-Lip with rabbit red blood cells (RBCs; Beijing Mutual Support Biotechnology Co., Ltd; Beijing, China). The RBCs were diluted to a 2% (v/v) concentration. 2.5 mL aliquot of the RBC suspension was mixed with an equal volume of ultrapure water, saline solution, or the designated test solutions. Ultrapure water and saline solution served as positive and negative controls, respectively. The samples were incubated at 37°C for 3 hours. RBC precipitates were observed and documented under a microscope. The absorbance of the supernatant was measured at 540 nm, and the hemolysis rate was calculated using the following equation.

$$\text{Hemolysis}(\%) = \frac{(A_{\text{sample}} - A_{\text{negativecontrol}})}{(A_{\text{positivecontrol}} - A_{\text{negativecontrol}})} \times 100\%$$

In vivo Brain Targetability Evaluation

Animal Studies

The study used 8-week-old male C57BL/6J mice weighing between 22–25 g, obtained from Beijing Weitong LiHua Co., Ltd (Beijing, China). The mice were maintained in an environment with a temperature of $22 \pm 1^\circ\text{C}$, relative humidity of $50 \pm 1\%$, and a 12-hour light/dark cycle. All animal procedures adhered to the Guiding Principles for the Use of

Laboratory Animals and were approved by the Institutional Animal Care and Use Committee of the Institute of Chinese Materia Medica, China Academy of Chinese Medical Sciences (2021B130).

The MPTP-induced PD model was established following a published protocol.³⁶ PD was induced by administering 30 mg/kg MPTP (dissolved in 0.9% saline) via intraperitoneal injection for five consecutive days.

In vivo Images of Liposomes in the PD Mice

The PD mice were randomly divided into two cohorts (n=6 per cohort): DiR@Lip and DiR@ANG-Lip. DiR-loaded PEG-Lip and ANG-Lip were administered intravenously via the tail vein at a dose of 1 mg DiR/kg. To compare the distribution of DiR@ANG-Lip between PD mice and normal mice, DiR@ANG-Lip was also injected into six C57BL/6J mice that did not receive MPTP. The mice were anesthetized and imaged at specific time points using an in vivo imaging system (Bruker, Germany). Two hours post-administration, a subset of animals (n=3) was euthanized, and vital organs including the heart, liver, spleen, lung, kidney, and brain were collected after transcardial perfusion with saline and subjected to imaging. For analysis of DiR@ANG-Lip distribution in the brain, the brain specimens were sectioned into 2 mm coronal slices and imaged.

Biodistribution Studies

The PD mice were randomly divided into three cohorts (n=5 per cohort): Free ECH, ECH@Lip, and ECH@ANG-Lip. Each cohort received an intravenous injection of either free ECH solution, ECH@Lip, or ECH@ANG-Lip, with a dosage of 24 mg ECH/kg. The mice were euthanized 1 hour after administration. Tissues (brain, heart, liver, spleen, lung, and kidney) were collected immediately following transcardial perfusion with saline and stored at -80°C until analysis.

For sample preparation, tissues (brain, heart, liver, spleen, lung, and kidney) were homogenized in 50% methanol (1 g: 4 mL) with 20 µL of antioxidant solution (2% ascorbic acid and 0.1% disodium edetate in water). 100 µL of the tissue homogenates were mixed with 100 µL of internal standard working solution, vortexed for 2 minutes, and then centrifuged at 15294 g at 4°C for 10 minutes. The supernatant was collected and evaporated to dryness under a gentle stream of nitrogen at room temperature. The residue was reconstituted in 100 µL of methanol, and centrifuged again at 15294 g at 4°C for 10 minutes. 2 µL of the supernatant above the sediment was examined using UPLC-MS/MS (UPLC-MS/MS conditions are detailed in the supplementary materials). The multiple reaction monitoring (MRM) transitions and optimized mass spectrometric parameters for ECH and the internal standards was presented in [Table S1](#).

In vivo Pharmacokinetics Analysis

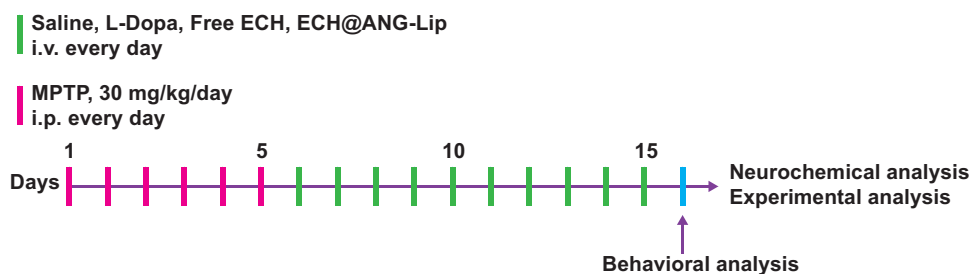
The ECH@ANG-Lip cohort received an intravenous dose of 13 mg/kg ECH@ANG-Lip via the tail vein, while the free ECH cohort received an equivalent dose of ECH dissolved in 0.9% saline. Plasma and brain samples were collected separately from treated mice (n=4). Plasma was collected from the orbital venous plexus at the following time points: 0.083, 0.25, 0.5, 0.75, 1, 1.5, 2, 4, 6, 12, and 24 hours post-administration. Brain samples were obtained after heart perfusion at the same time points. ECH concentrations in all samples were quantified using UPLC-MS/MS, following the same method used for ECH determination.

In vivo Therapeutic Effects

C57BL/6J mice were randomly assigned to five cohorts, with 12 mice per group. Cohort 1 (Control) received an injection of saline. Cohort 2 (MPTP) was given saline and MPTP at a dose of 30 mg/kg, dissolved in 0.9% saline, via intraperitoneal injection for five consecutive days. Cohort 3 (MPTP + L-Dopa) received both MPTP and levodopa (L-Dopa) at a dose of 4.95 mg/kg. Cohort 4 (MPTP + Free ECH) was administered MPTP along with free ECH at a dose of 13 mg/kg. Cohort 5 (MPTP + ECH@ANG-Lip) received MPTP and ECH@ANG-Lip, equivalent to 13 mg/kg of free ECH per body weight per administration. On day 16, behavioral tests were conducted ([Scheme 1](#)). Following the tests, mice were euthanized, and their hearts, livers, spleens, lungs, kidneys, and brains were collected after heart perfusion.

Behavioral Assays

On day 16, the open field test was conducted by placing the mice in the central area of a brightly illuminated open field arena measuring 50 cm × 50 cm × 50 cm for 10 minutes. The arena was divided into a central zone (30 cm × 30 cm) and



Scheme I Experiment protocol for animal treatment.

a peripheral zone. A video tracking system with ANY-maze software (ANY-maze 7.20, Stoelting Co., USA) recorded the mice's movements. Metrics such as total distance traveled, average speed, percentage of time spent in each zone, and time spent immobile in the center were analyzed.

Additionally, on day 16, a pole test was performed. Mice were carefully placed on top of a vertical wooden pole (diameter: 1.5 cm; height: 55 cm) with their heads facing upward. The time it took for the mice to descend to the floor (T-total) and the duration before they began their descent (T-turn) were recorded.

Determination of the Levels of Dopamine and Its Metabolites

Dopamine, 3,4-Dihydroxyphenylacetic acid (DOPAC), and homovanillic acid (HVA) levels in the striatum were quantified using UPLC-MS/MS. Briefly, striatal tissue was weighed and then homogenized with a homogenizer in a 10% trichloroacetic acid solution. The homogenate was centrifuged at 15294 g at 4°C for 10 minutes. 2 µL aliquot of the supernatant was then analyzed by UPLC-MS/MS (UPLC-MS/MS conditions are detailed in the supplementary materials). The MRM transitions and optimized mass spectrometric parameters for dopamine and its metabolites are listed in [Table S2](#).

Oxidative Stress Assay

The levels of superoxide dismutase (SOD), glutathione peroxidase (GSH-PX), and malondialdehyde (MDA) in the striatum were measured using SOD, GSH-PX, and MDA assay kit (Nanjing Jiancheng Bioengineering Institute, Nanjing, China), respectively. The striatum were homogenate with 1% triton (1 g/9 mL). Then, tissue homogenates were centrifuged at 15294 g under 4°C for 10 min. The supernatant was collected for quantitative analysis, which was performed according to the manufacturer's instructions for the reagent kits.

Immunohistochemical Staining

The coronal brain sections, with a thickness of 5 µm, were prepared utilizing a microtome. The sections were incubated overnight at 4°C with a rabbit polyclonal anti-tyrosine hydroxylase (TH) antibody (1:400) in PBS. Following this, the sections were treated with an HRP-conjugated rabbit anti-goat secondary antibody (1:200) and washed with PBS. The immune complexes were visualized using a diaminobenzidine solution. Microscopic digital images were acquired with a digital slide scanner (Pannoramic SCAN ii, 3DHISTECH). The immunoreactivity of TH in striatal fibers was analyzed using ImageJ software. For stereological counting of dopaminergic neurons in the substantia nigra, TH-positive cells with typical neuronal morphology were counted in every sixth section throughout the substantia nigra.

In vivo Biocompatibility

To assess the effects of ECH@ANG-Lip on various organs after 10 days of administration, pathological sections of the heart, liver, spleen, lung, and kidney from mice were examined. The tissues were fixed in 4% paraformaldehyde, then embedded, sectioned, stained with hematoxylin-eosin (HE), and sealed for microscopic observation to evaluate histological changes.

To determine if MPTP administration compromised the integrity of the BBB in mice, Evans blue (50 mg/kg) was injected intravenously into both MPTP-treated and untreated mice. The mice were euthanized 30 minutes post-injection.

Brain tissues were collected promptly, and Evans blue levels in the brain were quantified using a microplate reader (Thermo Fisher Scientific Inc., MA, USA) at 620 nm.

Statistical Analysis

Statistical analysis was conducted using GraphPad Prism software (Version 9.0.0). Data are presented as mean \pm standard deviation (SD). The Student's *t*-test was used to compare differences between two groups, while multiple comparisons were analyzed using One-way ANOVA followed by Dunnett's test. Statistical significance was defined as $p < 0.05$.

Results and Discussion

Optimization of the Modified Density of Angiopep-2 in Liposomes

To identify the optimal incubation time for cellular uptake, RhB@Lip and RhB@ANG-Lip (with ANG constituting 5% of SPC in RhB@ANG-Lip) were incubated with bEnd.3 cells for 30 to 120 minutes. Cells absorbed varying numbers of liposomes at varying times, but this difference became less apparent after uptake time exceeded 60 minutes (Figure 1A), which may be associated with the process of transcytosis in cells, specifically brain endothelial cells, which is a form of transcellular transport.^{37,38} The reasons may be twofold: the limitation of the number of receptors on the cell membrane, and on the other hand, the internalization and exocytosis of liposomes may tend to balance with the increase in time. Therefore, subsequent studies employed the 60-minute time point. To evaluate liposome internalization, bEnd.3 cells were exposed to RhB@ANG-Lip with ANG densities of 0%, 2%, 4%, 6%, and 8% for 60 minutes. Fluorescence microscopy and flow cytometry analyses were performed (Figure 1B–D). The fluorescence intensity in bEnd.3 cells

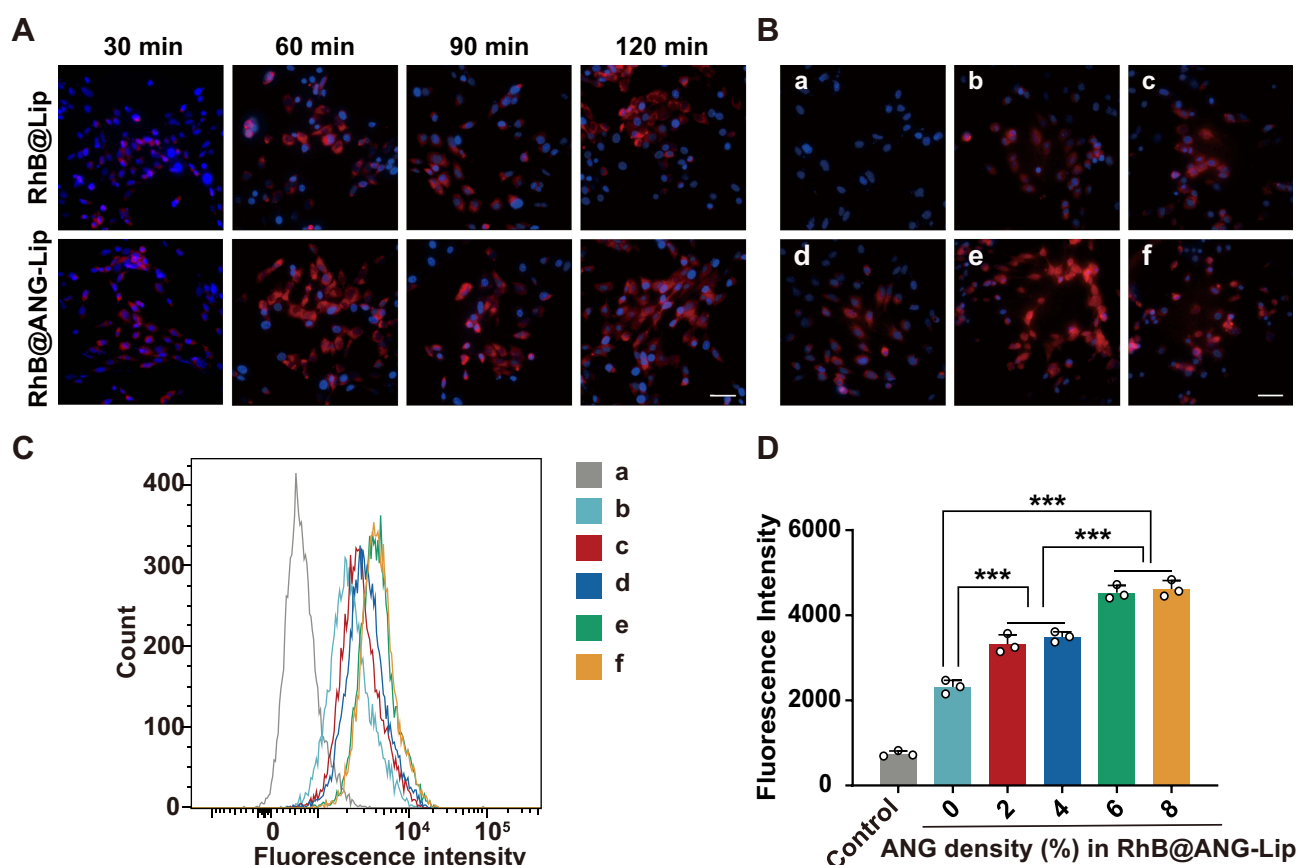


Figure 1 Optimization of the modified ANG density in RhB@ANG-Lip. (A) Fluorescence microscopy displaying liposome uptake following incubation for 30–120 minutes. (B) Fluorescence microscopy displaying RhB@ANG-Lip uptake with different ANG densities. Control (a); ANG density (0-, 2-, 4-, 6-, and 8%) in RhB@ANG-Lip (b-f). Liposomes appear in red; the nuclei are displayed in blue. Scale bars are 50 μ m. (C and D) The cellular uptakes of RhB@ANG-Lip with different ANG densities were quantified by flow cytometry. *** $p < 0.001$. Data are mean \pm SD (n=3).

increased with higher ANG densities, peaking at 6%. Thus, the optimal molar ratio of ANG to SPC in RhB@ANG-Lip for maximal cellular uptake was found to be 6%.

The NMR Spectroscopy

During the coupling process, the peptide ANG was successfully conjugated to the distal end of DSPE-PEG_{2K}-MAL via a Michael addition reaction between the cysteine residue and maleimide. To ensure effective presentation of the ANG-conjugated DSPE-PEG_{2K}-MAL on the liposome surface, a post-insertion technique was utilized.¹⁸ After conjugation, the characteristic peak of maleimide at 6.7 ppm in ANG-Lip vanished, and the characteristic peaks of ANG at 6.5 to 7.5 ppm were observed (Figure S1). The coupling efficiency was determined to be $89.99 \pm 0.45\%$.

Particle Size and Zeta Potential

The liposomes were initially characterized using laser scattering, which revealed a distinct bright “channel” in the solution, indicating a pronounced Tyndall effect (Figure 2A and B).³⁹ ECH@Lip exhibited an average size of 79.58 ± 1.18 nm (PDI 0.215 ± 0.008) and a zeta potential of -22.7 ± 0.59 mV. In contrast, ECH@ANG-Lip had an average size of 88.62 ± 0.20 nm (PDI 0.238 ± 0.006) and a zeta potential of 1.0 ± 0.17 mV (Figure 2C and D). After modification with ANG, the liposomes remained under 100 nm in size, facilitating their ability to cross the BBB.⁴⁰ The zeta potential of ECH@ANG-Lip changed significantly compared to unmodified ECH@Lip, which was caused by the coupling of ANG on the liposomes surface. On the surface of liposomes, part of the amino groups in ANG neutralize the negative charge of the phospholipid molecules, and the remaining free amino groups make the liposomes exhibit a positive charge.⁴¹ The results obtained from TEM indicated that the liposomes exhibited a predominantly spherical shape (Figure 2E and F).

The Encapsulation Efficiency and Loading Capacity

The addition of ANG did not significantly impact the encapsulation efficiency and loading capacity of ECH at a total lipid concentration of (14.16 ± 0.44) mM for all liposomes. The encapsulation efficiency was $55.20 \pm 0.12\%$ for ECH@Lip and $52.83 \pm 0.31\%$ for ECH@ANG-Lip. The loading capacity was $4.77 \pm 0.14\%$ for ECH@Lip and $4.25 \pm 0.12\%$ for ECH@ANG-Lip.

Stability Evaluation

By monitoring liposome particle size and encapsulation efficiency, we confirmed the stability of the liposomes in vitro (Figure 2G and H). Both ECH@Lip and ECH@ANG-Lip showed no significant increase in particle size after 48 hours in FBS (Figure 2I).

In vitro Drug Release Studies

The cumulative drug release curves for ECH@Lip and ECH@ANG-Lip were comparable. After 0.5 hours, the drug release rates were 10.93% for ECH@Lip and 15.02% for ECH@ANG-Lip. Both formulations reached their peak cumulative drug release at 4 hours, with rates of 68.99% for ECH@Lip and 69.86% for ECH@ANG-Lip (Figure 2J).

In vitro Blood-Brain Barrier Penetration Capability

To assess the capability of ECH@Lip and ECH@ANG-Lip to deliver ECH into the brain, a transwell assay using bEnd.3 cells as a BBB model was performed (Figure 3A).⁴² The CCK-8 assay demonstrated that ECH@Lip and ECH@ANG-Lip did not cause significant cytotoxicity in bEnd.3 cells (Figure 3B). The apparent permeability coefficient of fluorescein sodium was $6.92 \pm 3.92 \times 10^{-6}$ cm/s, confirming that the bEnd.3 monolayer was well established.⁴³ The transendothelial electrical resistance (TEER) for wells with ECH@Lip, ECH@ANG-Lip, and ECH@ANG-Lip+ANG remained above 200 $\Omega \cdot \text{cm}^2$ throughout the permeability assessment, indicating that the liposomes did not compromise the BBB (Figure 3C).⁴⁴ Thus, the in vitro BBB model was effectively established for investigating liposome transport. The Pe% for ECH@ANG-Lip was significantly higher than that for ECH@Lip at all time points (Figure 3D), indicating enhanced BBB penetration by ECH@ANG-Lip. However, pre-treating the cells with fresh ANG peptide for 1 hour partially inhibited the transport of ECH@ANG-Lip, suggesting that ANG peptide primarily mediates the uptake of ECH@ANG-Lip.

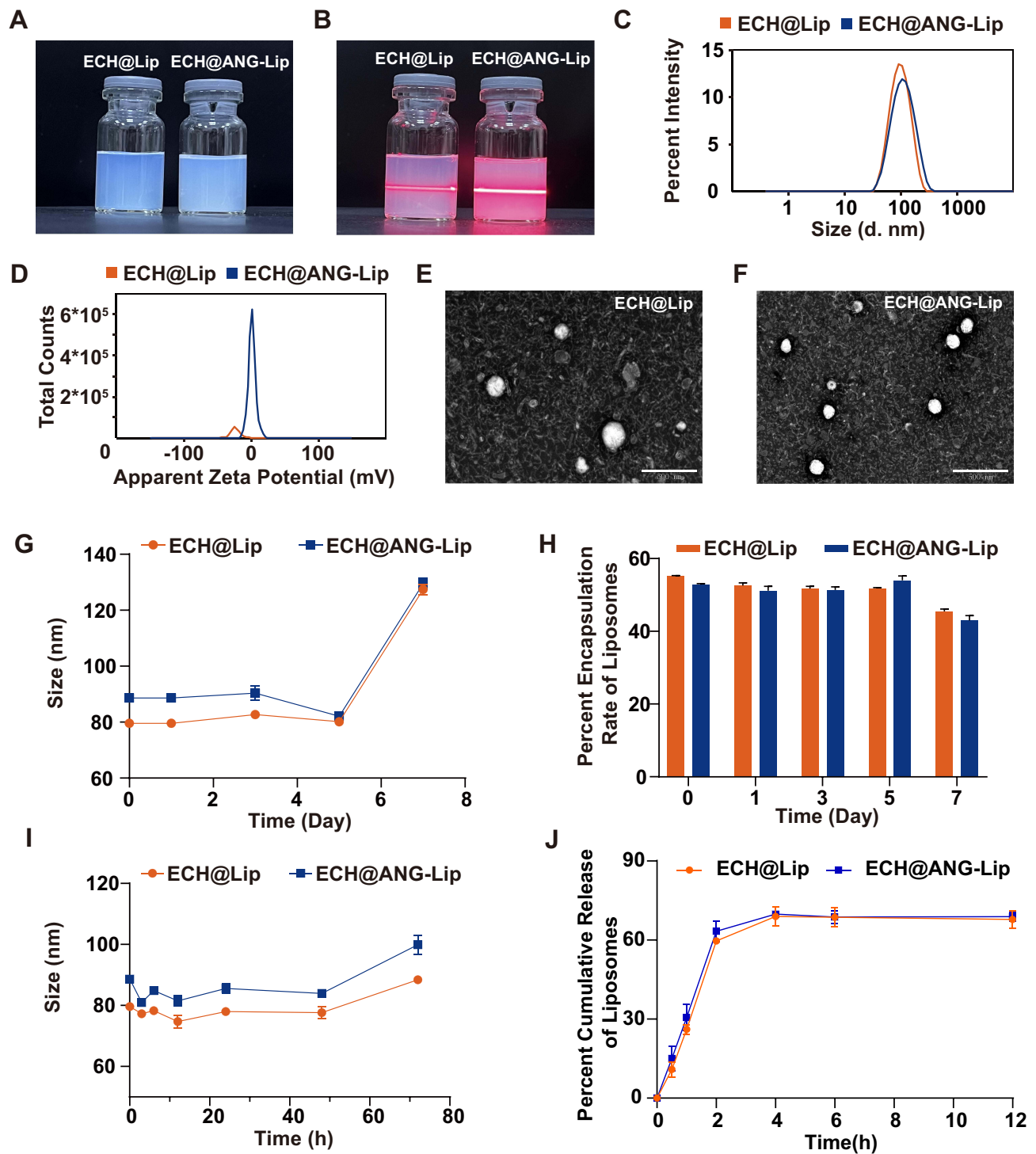


Figure 2 (A and B) Tindal effect of liposomes. (C and D) Size distribution graph and zeta potential distribution graph of ECH@Lip and ECH@ANG-Lip. (E and F) TEM analysis of liposomes. Scale bar 500 nm. (G) Stability of liposomes stored at 4°C for 7 days. (H) The encapsulation efficiency of liposomes stored at 4°C for 7 days. (I) The size of liposomes in FBS. (J) The release profiles of ECH solution and ECH-loaded liposomes in saline over 24 hours. Data are mean \pm SD (n=3).

Hemolysis Test

Ensuring optimal compatibility with RBCs is imperative for the successful in vivo implementation of drug delivery systems.⁴⁵ As shown in Figure 4A, there was a minimal release of hemoglobin observed in RBCs treated with liposomes, in contrast to RBCs treated with ultrapure water. Furthermore, the RBCs that were subjected to liposome treatment

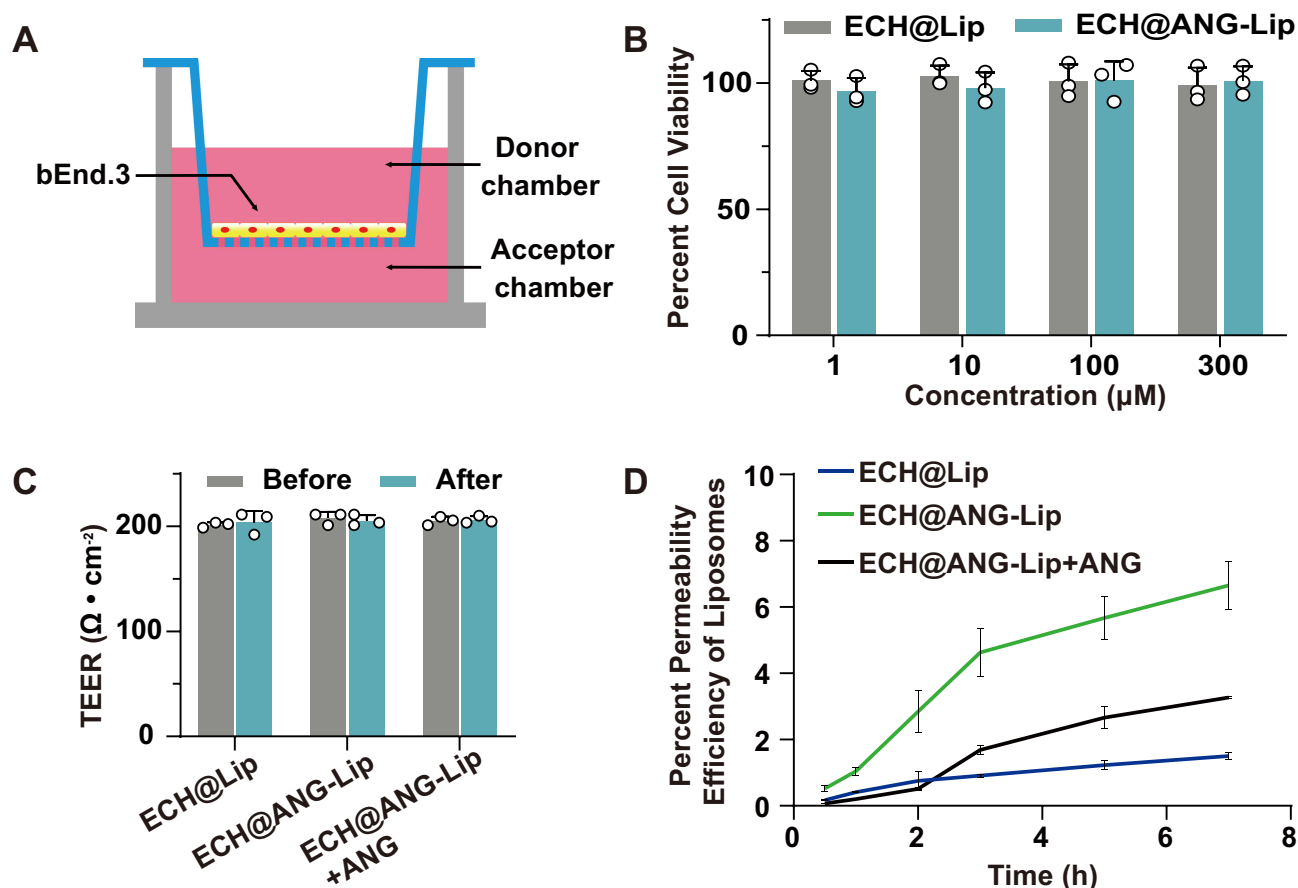


Figure 3 Assessment of brain targeting using in vitro model. **(A)** Schematic diagram of in vitro BBB model. **(B)** The viability of ECH@Lip and ECH@ANG-Lip on Bend.3 cells. **(C)** The TEER of the Bend.3 monolayer was assessed both prior to and subsequent to the treatments. **(D)** The echinacoside-loaded liposomes permeability through the BBB. Data are mean \pm SD ($n=3$).

exhibited a cellular morphology that was entirely comparable to that of the cohort treated with saline solution (Figure 4B). The hemolysis rates of all cohorts were less than 5% (Figure 4C), indicating that these liposomes were suitable for intravenous administration.⁴⁶ Interestingly, the hemolysis rate for ECH@ANG-Lip was higher than that for ECH@Lip. Following modification by ANG, the liposomes have transitioned from a negative to a positive zeta potential, leading to increased damage to red blood cells.⁴⁷

In vivo Brain Targetability Evaluation

To assess the brain targeting of DiR@ANG-Lip, a fluorescence imaging system was used for in vivo analysis. A strong fluorescence signal was observed in the brains of PD and C57BL/6J mice treated with DiR@ANG-Lip following intravenous administration. In contrast, mice treated with DiR@Lip exhibited lower fluorescence signals in the brain (Figure 5A). To confirm the precise localization of liposomes within the brain, ex vivo imaging techniques were employed to obtain images of extracted brain and DiR@ANG-Lip was well distributed in the brain (Figure 5B); the highest signals were localized to the thalamic region (c3-c5) (Figure 5C). This indicates that the ANG-Lip formulation has improved brain distribution due to the ANG-mediated endocytosis mechanism. Besides brain targeting, DiR@ANG-Lip nanoparticles also showed increased fluorescence signals in the liver, lung, and kidney (Figure 5D). The presence of the blood-brain barrier necessitates that substances in the bloodstream are transported by channel proteins on the brain microvascular endothelial cells to enter brain tissue.⁴⁸ By coupling targeting proteins to the liposome surface, we significantly enhanced liposome distribution in the brain. However, the liver is typically a major site of nanoparticle accumulation due to its large blood volume and complex vascular system, which facilitates nanoparticle distribution.⁴⁹

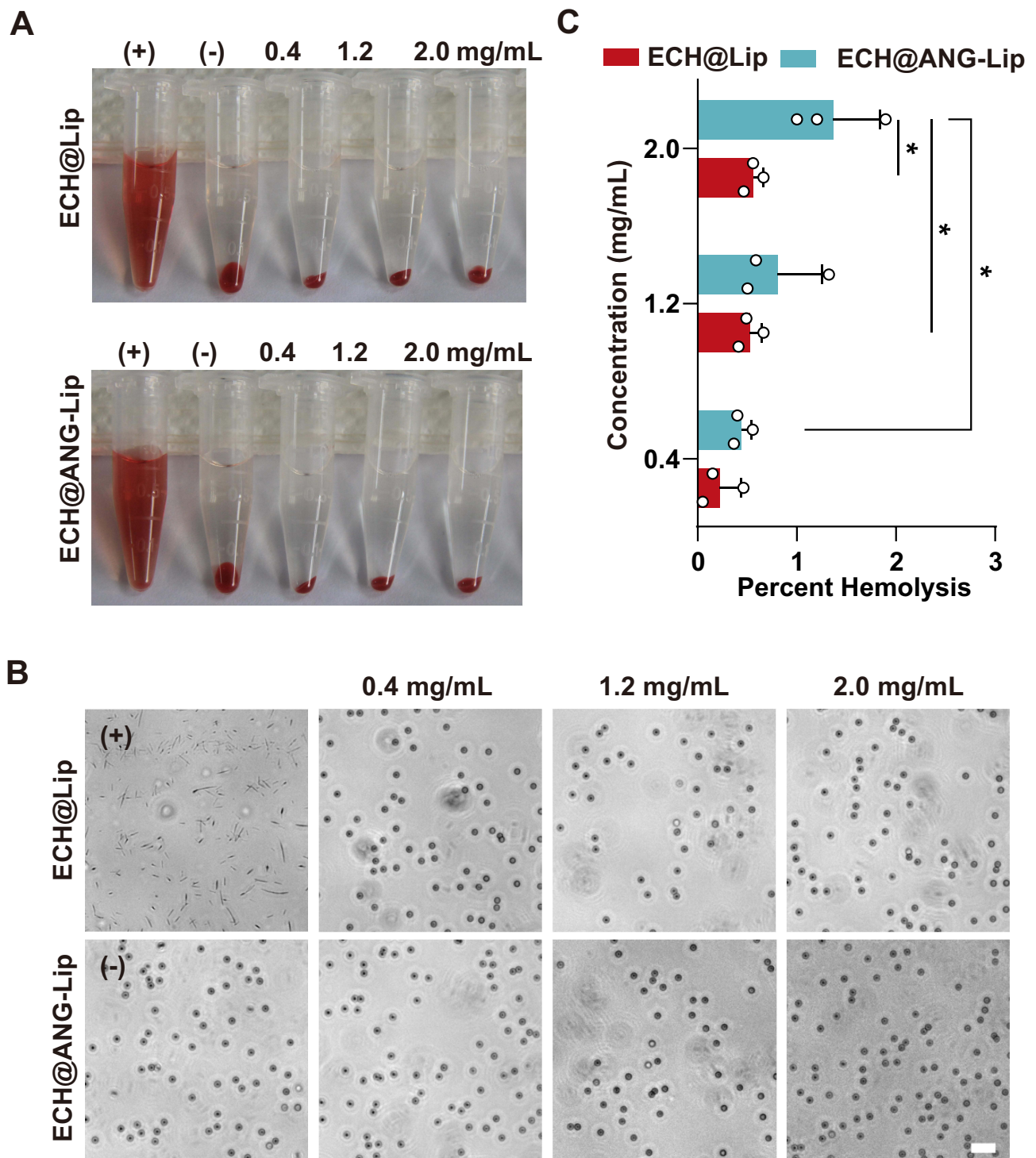


Figure 4 Hemolysis test. **(A)** Photographs. **(B)** Microscope images. **(C)** Hemolysis rates of RBCs from rabbits treated by liposomes. * $p < 0.05$ were considered statistically significant. Data are shown as mean \pm SD ($n=3$).

After ANG coupling, the surface charge of liposomes changed from -22.7 ± 0.59 mV to 1.0 ± 0.17 mV, making them more positively charged and more readily captured by macrophages in the lungs, liver, and spleen. Therefore, ANG-Lip showed increased distribution in these organs.⁵⁰ To further validate the efficacy of ANG-Lip in delivering ECH to the brain, a quantitative analysis of ECH distribution was performed using UPLC-MS/MS. The ECH concentration in the brain of the ECH@ANG-Lip cohort (230.22 ± 33.76 ng/g) was significantly higher compared to other cohorts (11.4-fold

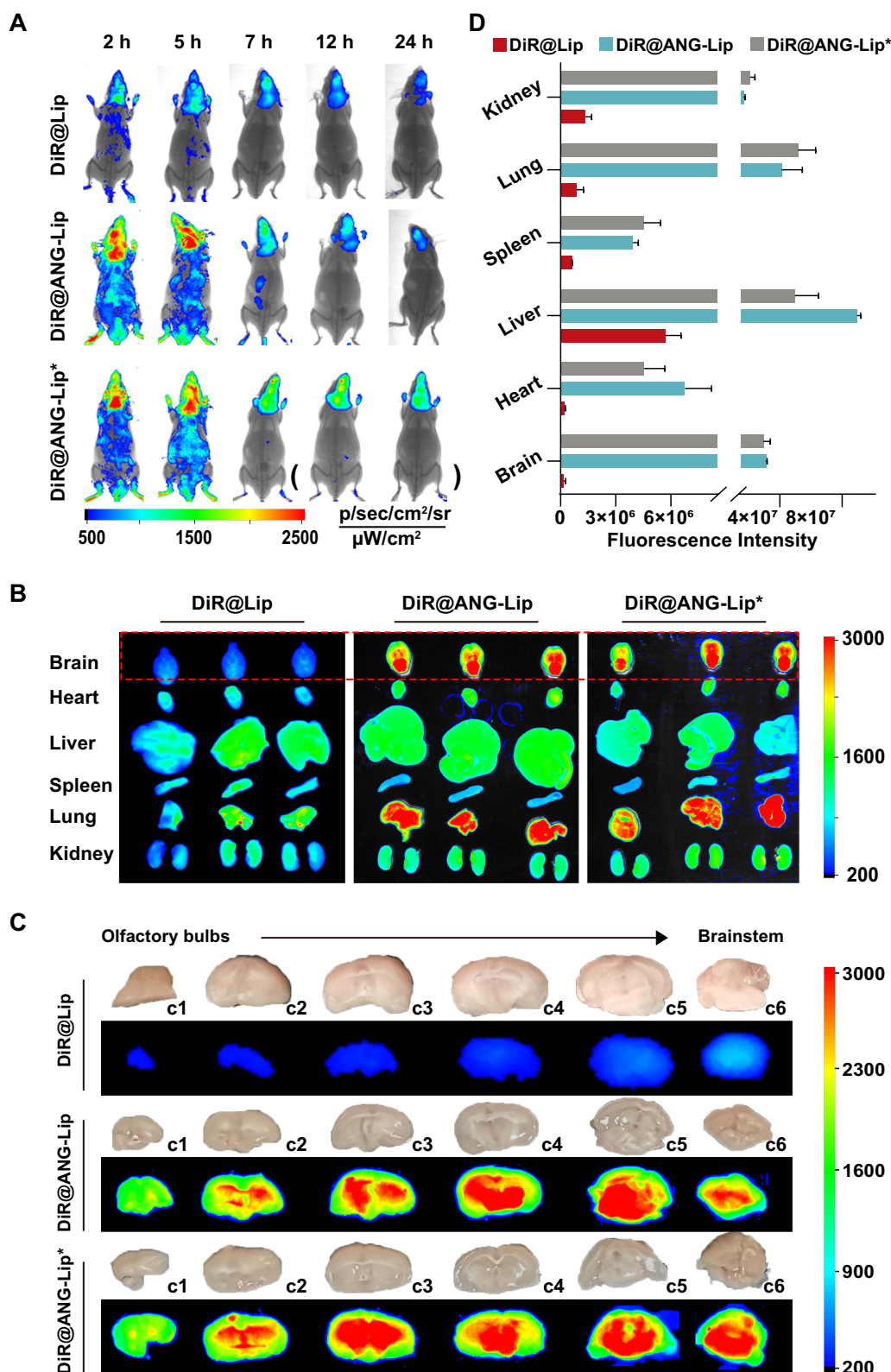


Figure 5 (A) In vivo imaging of different liposome-loaded DiR in PD mice. (B) Ex vivo imaging of the major organs from mice treated intravenously with DiR@Lip and DiR@ANG-Lip for 2 hours. (C) Ex vivo imaging of brain sections from mice treated intravenously with DiR@Lip and DiR@ANG-Lip for 2 hours. *This cohort of C57BL/6j mice without MPTP injection. (D) Semi-quantitative analysis of fluorescence signal of the major organs from A. Data are represented as mean \pm SD ($n=3$).

higher than the free ECH cohort, $p < 0.001$; 2.3-fold higher than the ECH@Lip cohort, $p < 0.001$) (Figure 6). Additionally, ECH concentrations in all tissues of the ECH@Lip and ECH@ANG-Lip cohorts increased significantly at 1 hour compared to the free ECH cohort, demonstrating that liposomes effectively deliver ECH to the brain, with ANG-Lip providing superior delivery efficiency.

In vivo Pharmacokinetics Analysis

Pharmacokinetic analysis was conducted to evaluate the in vivo characteristics of ECH@ANG-Lip. The plasma concentration-time curve and noncompartmental pharmacokinetic parameters are shown in Figure 7A and Table 1, respectively. Intravenous administration of ECH@ANG-Lip significantly enhanced the half-life ($T_{1/2}$) to 1.242 ± 0.165 hours, peak plasma concentration (C_{max}) to 26.826 ± 3.184 $\mu\text{g/mL}$, and mean residence time (MRT_{0-t}) to 6.367 ± 0.452 hours, indicating a slower elimination rate compared to free ECH. Additionally, ECH@ANG-Lip significantly increased the area under the curve (AUC_{0-t}) to 167.104 ± 17.250 $\text{h} \cdot \mu\text{g/g}$, compared to 3.501 ± 0.733 $\text{h} \cdot \mu\text{g/g}$ for free ECH. These results demonstrate a substantial improvement in the bioavailability of ECH when delivered via the ECH@ANG-Lip nanoplatform.

The brain concentration-time curve following intravenous administration (Figure 7B) was also measured, and pharmacokinetic parameters were calculated (Table 1). The ECH@ANG-Lip cohort exhibited a C_{max} approximately 7.89 times higher than the free ECH cohort. Moreover, the $T_{1/2}$ in the ECH@ANG-Lip group was extended to $7.787 \pm$

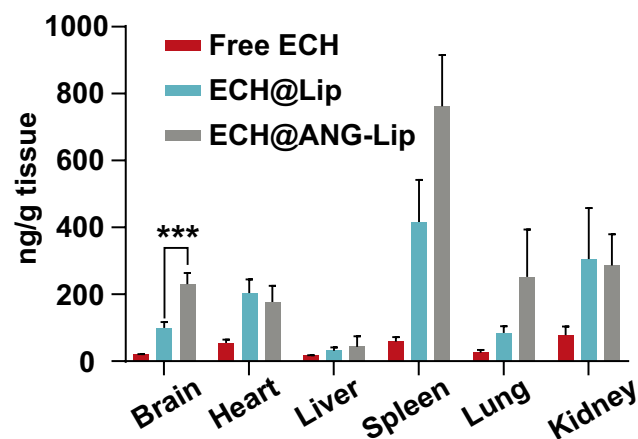


Figure 6 ECH dispersion in mouse organs 1 hour following intravenous injection. Compared with the ECH@Lip cohort: *** $p < 0.001$. Data are shown as mean \pm SD ($n=5$).

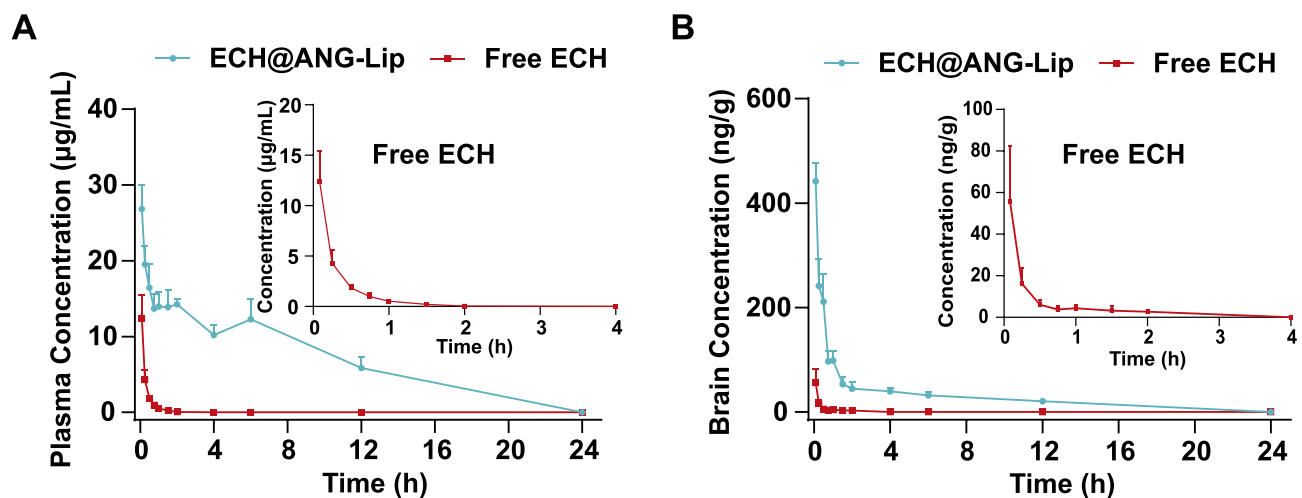


Figure 7 In vivo pharmacokinetics analysis after treated with ECH or ECH@ANG-Lip. (A) Plasma and (B) brain concentration-time profiles. Data are presented as means \pm SD ($n=4$).

Table I Pharmacokinetic Parameters in the Plasma and Brain (n=4)

Parameters	Free ECH	ECH@ANG-Lip
Plasma		
$T_{1/2}$ (h)	0.380 ± 0.015	1.242 ± 0.165***
C_{max} (µg/mL)	12.422 ± 3.041	26.826 ± 3.184***
AUC_{0-t} (h µg/mL)	3.501 ± 0.733	167.104 ± 17.250***
MRT_{0-t} (h)	0.349 ± 0.003	6.367 ± 0.452***
Brain		
$T_{1/2}$ (h)	0.562 ± 0.114	7.787 ± 1.346***
C_{max} (µg/g)	0.056 ± 0.027	0.442 ± 0.036***
AUC_{0-t} (h µg/g)	0.017 ± 0.005	0.570 ± 0.082***
MRT_{0-t} (h)	0.509 ± 0.095	3.605 ± 0.247***

Notes: Data are presented as means ± SD. *** $p < 0.001$ vs the free ECH cohort.

1.346 hours, which is 13.86 times longer than that of free ECH. Furthermore, the AUC_{0-t} and MRT_{0-t} values for the ECH@ANG-Lip cohort increased by 33.53-fold and 7.08-fold, respectively, compared to the free ECH cohort.

In vivo Therapeutic Efficacy

To assess the motor behavior and exercise capacity of mice, we conducted open-field tests. Compared to the control cohort, MPTP-treated mice showed a marked reduction in movement within the central area of the arena (Figure 8A). Treatment with L-Dopa and ECH@ANG-Lip significantly improved movement within this central area. Additionally, L-Dopa and ECH@ANG-Lip treatment increased the total distance traveled, average speed, and percentage of time spent in the center, while decreasing the time spent immobile, compared to the MPTP-treated mice. Pole tests, which measure bradykinesia based on the time to turn (T-turn) and time to reach the bottom (T-total), revealed that both L-Dopa and ECH@ANG-Lip treatments significantly reduced T-turn and T-total times compared to the MPTP-treated cohort (Figure 8A). These results suggest that ECH@ANG-Lip can mitigate MPTP-induced behavioral impairments.

MPTP is known to specifically target dopaminergic neurons, leading to dopamine depletion and decreased metabolites in the striatum.³⁶ UPLC-MS/MS analysis showed dopamine levels in the control, MPTP, L-Dopa, free ECH, and ECH@ANG-Lip cohorts were 2.52 ± 0.49 , 0.95 ± 0.15 , 1.27 ± 0.09 , 1.27 ± 0.36 , and 1.64 ± 0.20 ng/mg of wet striatum tissue, respectively (Figure 8B). The MPTP cohort exhibited a significant decrease in dopamine levels (2.65-fold reduction, $p < 0.01$ compared to the control). The ECH@ANG-Lip cohort showed a notable increase in dopamine levels (1.72-fold, $p < 0.001$ compared to the MPTP cohort), reaching 65.08% of the levels found in the control cohort. L-Dopa administration also significantly increased dopamine levels compared to the MPTP cohort ($p < 0.05$). However, ECH@ANG-Lip treatment resulted in a greater increase in dopamine levels than L-Dopa. Both L-Dopa and ECH@ANG-Lip treatments significantly elevated DOPAC levels in MPTP mice compared to the MPTP cohort (L-Dopa: 1.59-fold increase, $p < 0.05$; ECH@ANG-Lip: 1.50-fold increase, $p < 0.05$). HVA levels also improved significantly with both treatments (L-Dopa: 1.63-fold increase, $p < 0.01$; ECH@ANG-Lip: 1.46-fold increase, $p < 0.05$). Many neurotransmitter pathways are affected in PD, and dopamine deficits are often considered a characteristic pathology of the disease.^{51–53} These findings indicate that ECH@ANG-Lip significantly enhances dopamine levels in the striatum, suggesting a strong therapeutic effect on MPTP-induced PD mice.

Immunohistochemical analysis for TH was used to examine dopaminergic fibers in the striatum and dopaminergic neurons in the substantia nigra. MPTP administration led to a significant reduction in TH immunoreactivity in the

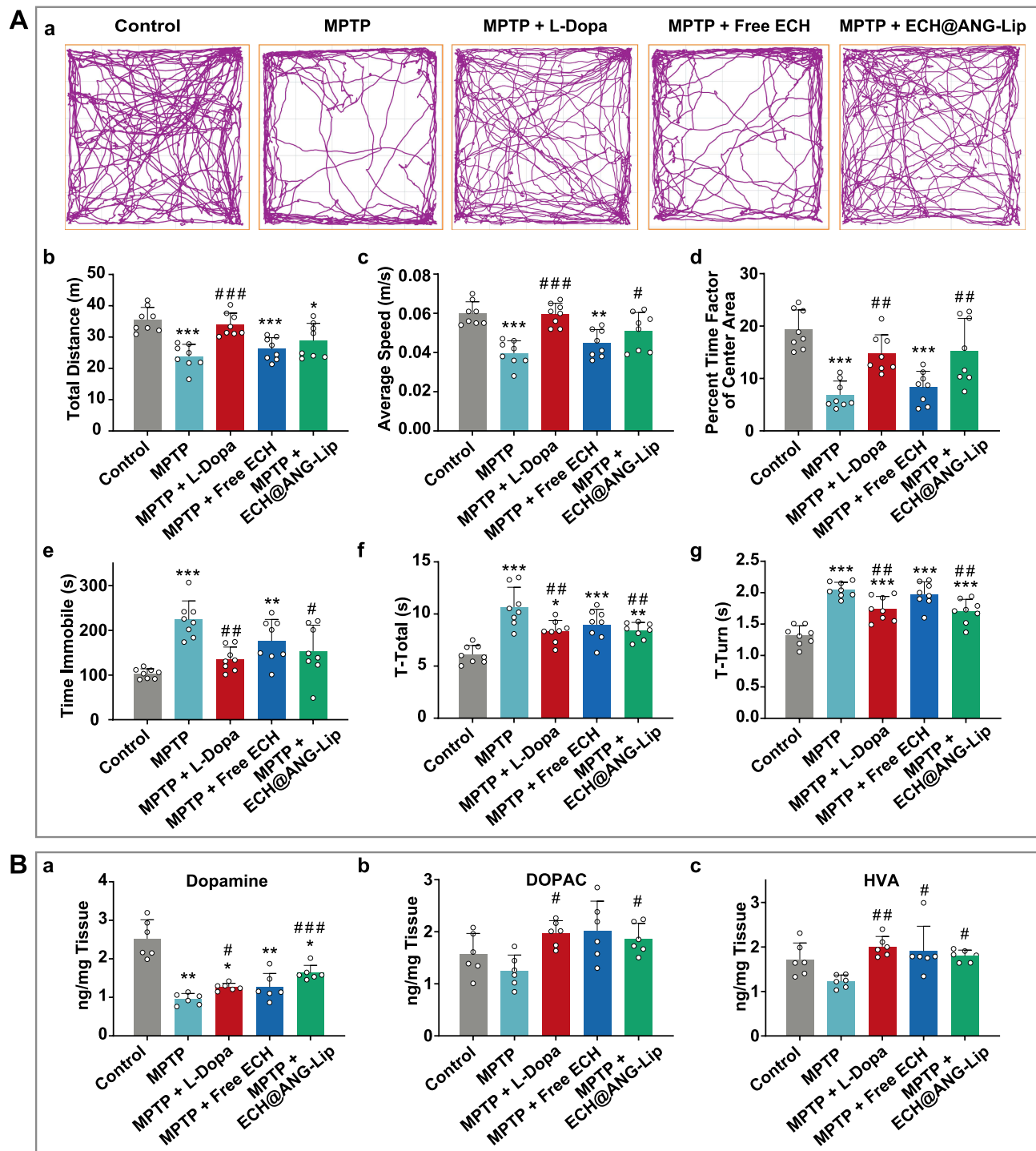


Figure 8 (A) Open-field test and Pole test. (a) Representative traces of mice pattern activity (purple) were obtained through video tracking. The total traveled distance (b), average speed (c), percentage of time in center (d), time immobile (e), and pole test (f and g) of mice in all cohorts. Data are mean \pm SD (n=8). **(B)** The level of dopamine (a), DOPAC (b) and HVA (c) in the striatum. Data are mean \pm SD (n=6). Compared with the control cohort: * $p < 0.05$, ** $p < 0.01$ and *** $p < 0.001$. Compared with the MPTP cohort: # $p < 0.05$, ## $p < 0.01$ and ### $p < 0.001$.

striatum. This reduction was effectively counteracted by L-Dopa and ECH@ANG-Lip treatments, with ECH@ANG-Lip showing the most pronounced neuroprotective effect compared to free ECH and L-Dopa. The ECH@ANG-Lip cohort had a higher density of TH-positive dopaminergic fibers in the striatum (Figure 9). Similarly, TH-positive neuron counts in the substantia nigra were reduced in the MPTP cohort but partially restored following L-Dopa and ECH@ANG-Lip

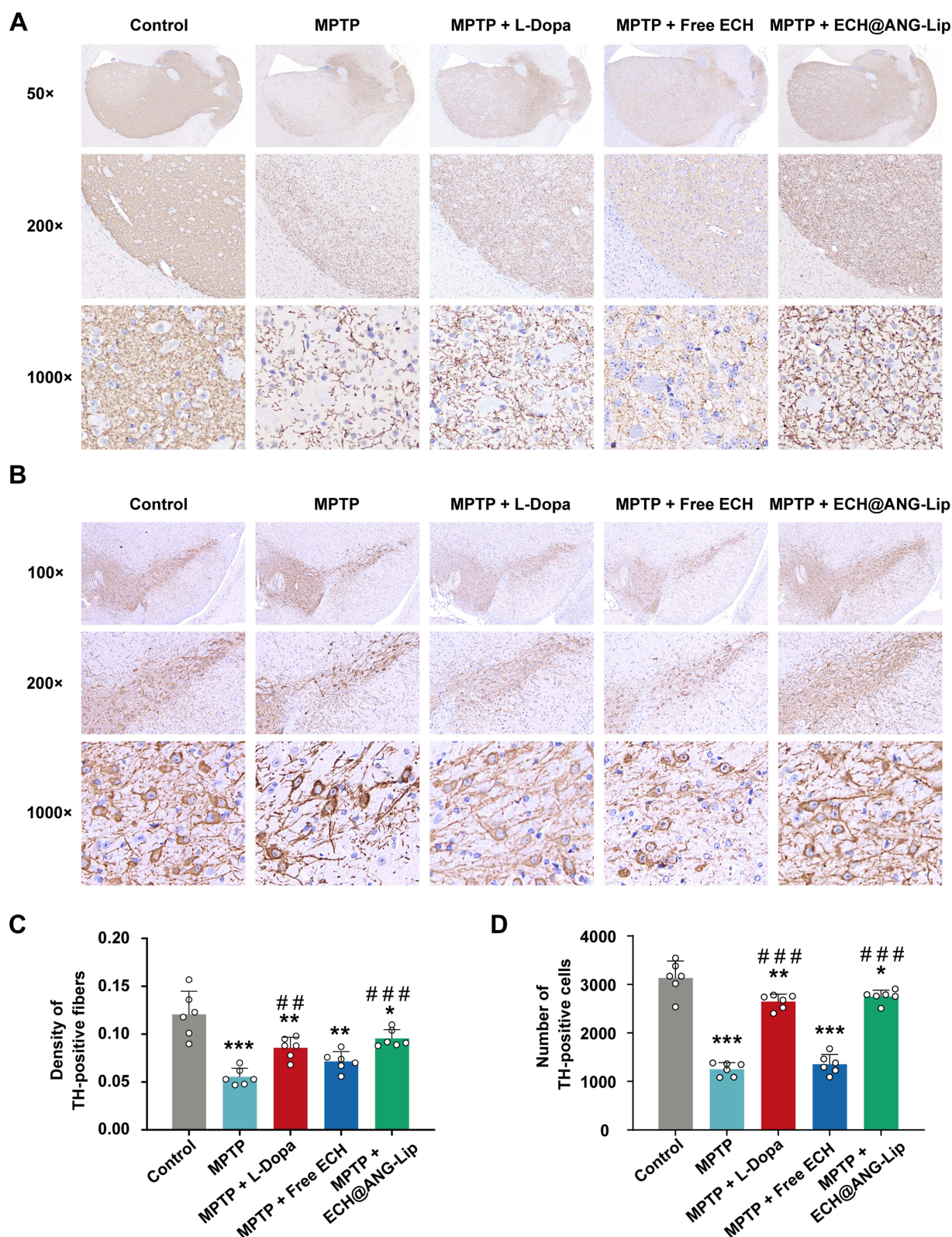


Figure 9 (A) Immunostaining of TH-positive fibers in the striatum. (B) Immunostaining of TH-positive dopaminergic neurons. Quantitative analysis for TH-positive fibers (C) and TH-positive dopaminergic neurons (D). Compared with the control cohort: * $p < 0.05$, ** $p < 0.01$ and *** $p < 0.001$. Compared with the MPTP cohort: # $p < 0.01$ and ### $p < 0.001$. Data are mean \pm SD ($n=6$).

treatments (Figure 9). Interestingly, free ECH did not provide significant neuroprotection compared to the MPTP cohort, which contradicts previous research findings.^{11,54} We guess that the low concentration of ECH in the brains of mice in the free ECH cohort rendered the treatment ineffective. Therefore, if the intragastric administration of a similar dosage of ECH can achieve good neuroprotective effects, it is plausible that ECH may confer neuroprotective benefits through the modulation of intestinal flora imbalance.^{11,55,56}

MPTP has been reported to cause oxidative stress leading to the death of dopaminergic neurons.⁵⁷ The exact contribution of oxidative stress for progressing of neurodegenerative disorders remains uncertain, but its impact on neurodegeneration is undeniable.^{58,59} Compared to the control cohort, the MPTP cohort exhibited significantly reduced levels of GSH-PX and SOD in the striatum, along with increased MDA levels (Figure 10). This indicates impaired antioxidant capacity and increased oxidative stress. Both L-Dopa and ECH@ANG-Lip treatments significantly elevated GSH-PX and SOD levels while reducing MDA levels, indicating improved oxidative stress management.

In vivo Biocompatibility

Histological examination of the main organs from mice administered the treatments for 10 days revealed no significant abnormalities (Figure 11). In the heart, cardiac muscle fibers were well-organized, evenly stained, with visible intercalated discs and transverse striae, and the nuclei appeared oval and centrally located. There was no evidence of interstitial vessel dilation or narrowing, nor any inflammatory cell infiltration. In the liver, hepatocyte cords were orderly, and hepatic sinuses were clearly visible. The interlobular arteries, veins, and bile ducts in the confluent area showed no signs of dilation, hyperplasia, luminal narrowing, inflammation, or fibrous tissue proliferation. The spleen showed an intact peritoneum with no observed thickening. The splenic sinuses did not show dilation, and there were no abnormal changes in the size of splenic vesicles; the red-to-white marrow ratio remained approximately normal. In the lungs, bronchi appeared normal, and the alveolar walls were composed of a single layer of epithelium with a clear structure. The interstitium, including intrapulmonary connective tissue and blood vessels, showed no significant inflammatory changes. The kidneys exhibited an intact surface with a distinct corticomedullary division. Glomeruli in the cortex were evenly distributed, with a normal number of cells in both glomeruli and stroma. Renal tubule epithelial cells were rounded and full, with a neatly arranged brush border. The medulla showed no significant abnormalities. Additionally, treated mice did not exhibit noticeable decreases in body weight (Figure S2).

Evans blue injections into MPTP-treated and control mice revealed no significant differences in Evans blue levels in brain tissue, with no accumulation observed in the brain (Figure S3). This suggests that MPTP administration did not compromise BBB integrity.⁶⁰

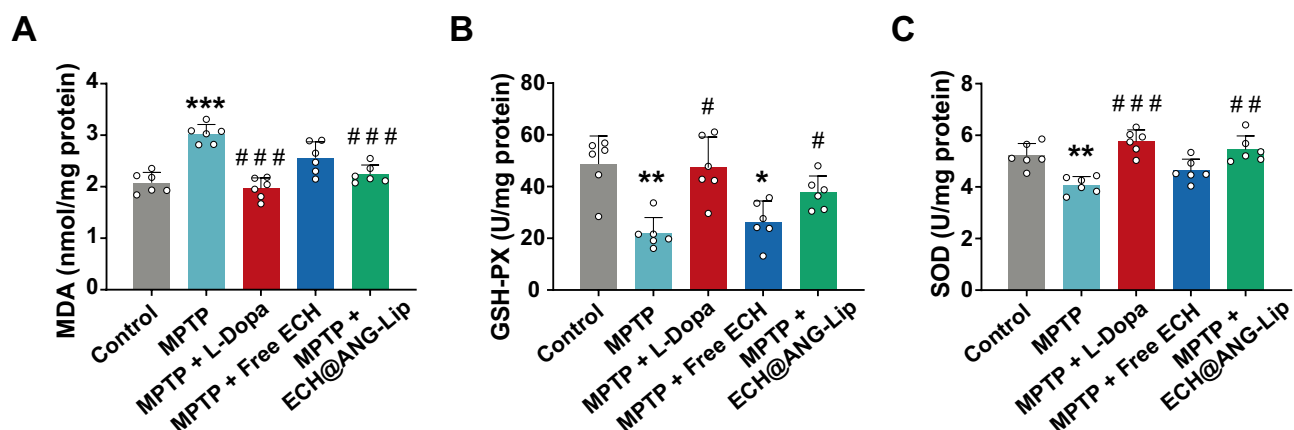


Figure 10 (A) Levels of MDA in the striatum of various treatment cohorts. (B) Levels of GSH-PX in the striatum of different treatment cohorts. (C) Total SOD levels in the striatum of various treatment cohorts. Compared with the control cohort: * $p < 0.05$, ** $p < 0.01$ and *** $p < 0.001$. Compared with the MPTP cohort: # $p < 0.05$, ## $p < 0.01$ and ### $p < 0.001$. Data are mean \pm SD ($n=6$).

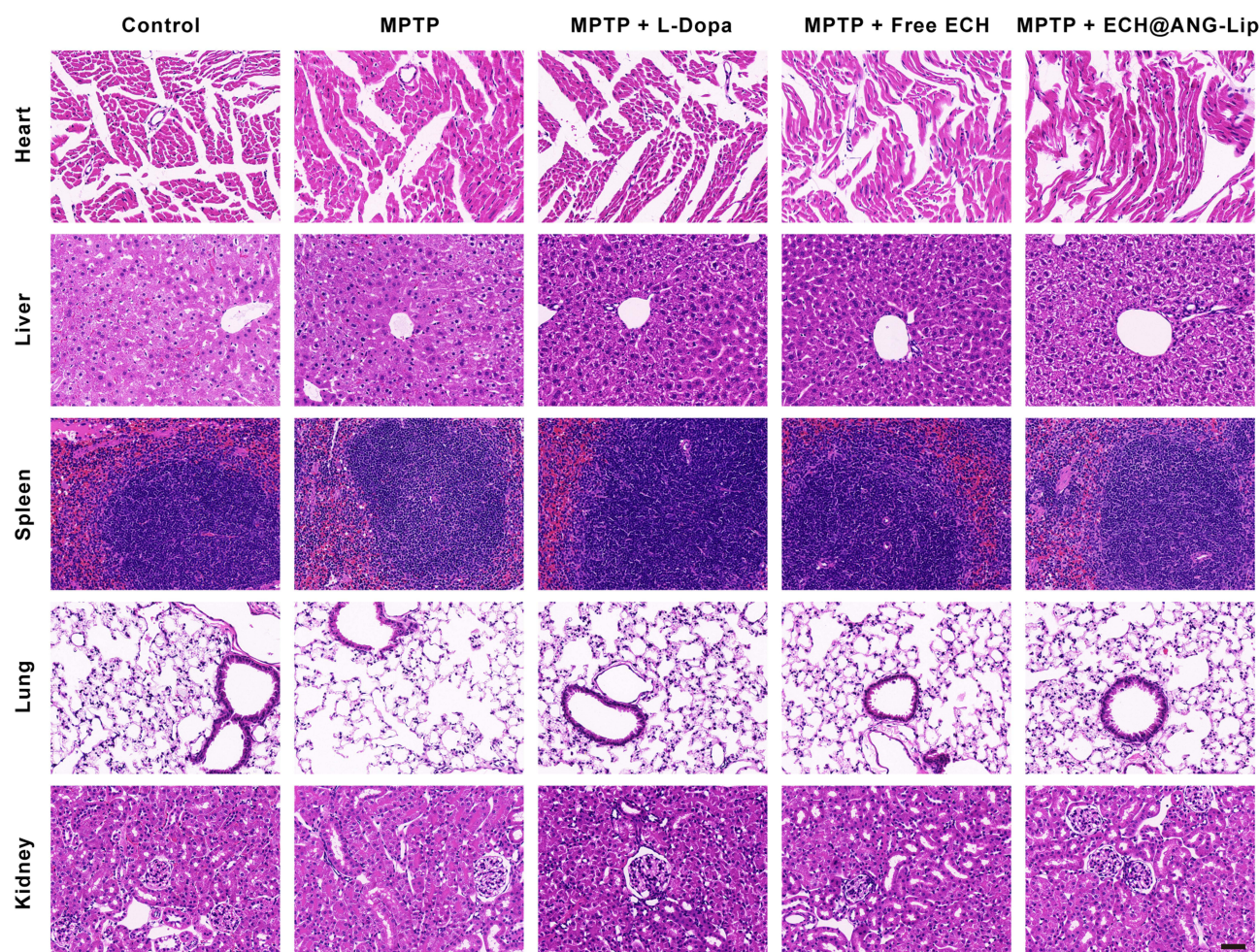


Figure 11 In vivo biocompatibility analysis. The H&E staining of heart, liver, spleen, lung, and kidney. Scale bar = 50 μ m. (n = 6).

Conclusion

In summary, we developed and validated a biocompatible liposome modified with the BBB-penetrating peptide ANG to deliver ECH into the brain for PD treatment. This study thoroughly demonstrates the enhanced BBB-targeting ability and efficacy of ANG-conjugated liposomes compared to other methods. Therefore, ANG-conjugated liposomes represent a promising carrier for brain drug delivery and hold significant potential for treating various neurodegenerative diseases.

Acknowledgments

We extend our gratitude to Associate Researcher Yu Zhao for her valuable review and suggestions. We also thank Associate Researcher Qinghe Zhao and Dr. Lu Liu for their insightful comments and recommendations. Our appreciation goes to Nanjing KEW Biotechnology Co., Ltd (Nanjing, China) for their support with the behavioral experiments, and to Global Biotech Inc. (Suzhou, China) for providing the ANY maze software used in this study. Additionally, we acknowledge the Home for Researchers (www.home-for-researchers.com) for their support.

Funding

The authors express their gratitude for the support received from the Scientific and Technological Innovation Project of China Academy of Chinese Medical Sciences (CI2021A04303) and the Outstanding Young Science and Technology Talent Project of China Academy of Chinese Medical Sciences (ZZ14-YQ-024).

Disclosure

The authors report no conflicts of interest in this work.

References

1. Tansey MG, Wallings RL, Houser MC, Herrick MK, Keating CE, Joers V. Inflammation and immune dysfunction in Parkinson disease. *Nat Rev Immunol*. 2022;22(11):657–673. doi:10.1038/s41577-022-00684-6
2. Bloem BR, Okun MS, Klein C. Parkinson's disease. *Lancet*. 2021;397(10291):2284–2303. doi:10.1016/s0140-6736(21)00218-x
3. Surmeier DJ, Obeso JA, Halliday GM. Selective neuronal vulnerability in Parkinson disease. *Nat Rev Neurosci*. 2017;18(2):101–113. doi:10.1038/nrn.2016.178
4. Michel PP, Hirsch EC, Hunot S. Understanding dopaminergic cell death pathways in Parkinson disease. *Neuron*. 2016;90(4):675–691. doi:10.1016/j.neuron.2016.03.038
5. Kam TI, Mao X, Park H, et al. Poly(ADP-ribose) drives pathologic α -synuclein neurodegeneration in Parkinson's disease. *Science*. 2018;362(6414):1–27. doi:10.1126/science.aat8407
6. Qian H, Kang X, Hu J, et al. Reversing a model of Parkinson's disease with in situ converted nigral neurons. *Nature*. 2020;582(7813):550–556. doi:10.1038/s41586-020-2388-4
7. Armstrong MJ, Okun MS. Diagnosis and treatment of Parkinson disease: a review. *JAMA*. 2020;323(6):548–560. doi:10.1001/jama.2019.22360
8. Espay AJ, Morgante F, Merola A, et al. Levodopa-induced dyskinesia in Parkinson disease: current and evolving concepts. *Ann Neurol*. 2018;84(6):797–811. doi:10.1002/ana.25364
9. Saranza G, Lang AE. Levodopa challenge test: indications, protocol, and guide. *J Neurol*. 2021;268(9):3135–3143. doi:10.1007/s00415-020-09810-7
10. Hornykiewicz O. A brief history of levodopa. *J Neurol*. 2010;257(Suppl 2):S249–252. doi:10.1007/s00415-010-5741-y
11. Zhao Q, Yang X, Cai D, et al. Echinacoside Protects Against MPP(+)-Induced Neuronal Apoptosis via ROS/ATF3/CHOP Pathway Regulation. *Neurosci Bull*. 2016;32(4):349–362. doi:10.1007/s12264-016-0047-4
12. Zeng KW, Wang JK, Wang LC, et al. Small molecule induces mitochondrial fusion for neuroprotection via targeting CK2 without affecting its conventional kinase activity. *Signal Transduct Target Ther*. 2021;6(1):71. doi:10.1038/s41392-020-00447-6
13. Jia C, Shi H, Wu X, Li Y, Chen J, Tu P. Determination of echinacoside in rat serum by reversed-phase high-performance liquid chromatography with ultraviolet detection and its application to pharmacokinetics and bioavailability. *J Chromatogr B Analyt Technol Biomed Life Sci*. 2006;844(2):308–313. doi:10.1016/j.jchromb.2006.07.040
14. Zheng Q, Tang Y, Hu PY, et al. The influence and mechanism of ligustilide, senkyunolide I, and senkyunolide A on echinacoside transport through MDCK-MDR1 cells as blood-brain barrier in vitro model. *Phytother Res*. 2018;32(3):426–435. doi:10.1002/ptr.5985
15. Peng H, Li Y, Ji W, et al. Intranasal administration of self-oriented nanocarriers based on therapeutic exosomes for synergistic treatment of Parkinson's disease. *ACS Nano*. 2022;16(1):869–884. doi:10.1021/acsnano.1c08473
16. Sun M, Li Y, Zhang W, et al. Allomelanin-based biomimetic nanotherapeutics for orthotopic glioblastoma targeted photothermal immunotherapy. *Acta Biomater*. 2023;166:552–566. doi:10.1016/j.actbio.2023.05.037
17. Yin T, Yang L, Liu Y, Zhou X, Sun J, Liu J. Sialic acid (SA)-modified selenium nanoparticles coated with a high blood-brain barrier permeability peptide-B6 peptide for potential use in Alzheimer's disease. *Acta Biomater*. 2015;25:172–183. doi:10.1016/j.actbio.2015.06.035
18. Qu M, Lin Q, He S, et al. A brain targeting functionalized liposomes of the dopamine derivative N-3,4-bis(pivaloyloxy)-dopamine for treatment of Parkinson's disease. *J Control Release*. 2018;277:173–182. doi:10.1016/j.jconrel.2018.03.019
19. Kim HR, Cho HB, Lee S, Park JI, Kim HJ, Park KH. Fusogenic liposomes encapsulating mitochondria as a promising delivery system for osteoarthritis therapy. *Biomaterials*. 2023;302:122350. doi:10.1016/j.biomaterials.2023.122350
20. Raza F, Evans L, Motallebi M, et al. Liposome-based diagnostic and therapeutic applications for pancreatic cancer. *Acta Biomater*. 2023;157:1–23. doi:10.1016/j.actbio.2022.12.013
21. Saraiva C, Praça C, Ferreira R, Santos T, Ferreira L, Bernardino L. Nanoparticle-mediated brain drug delivery: overcoming blood-brain barrier to treat neurodegenerative diseases. *J Control Release*. 2016;235:34–47. doi:10.1016/j.jconrel.2016.05.044
22. Abbott NJ, Rönnbäck L, Hansson E. Astrocyte-endothelial interactions at the blood-brain barrier. *Nat Rev Neurosci*. 2006;7(1):41–53. doi:10.1038/nrn1824
23. Zhi K, Raji B, Nookala AR, et al. PLGA nanoparticle-based formulations to cross the blood-brain barrier for drug delivery: from R&D to cGMP. *Pharmaceutics*. 2021;13(4):111–127. doi:10.3390/pharmaceutics13040500
24. Katila N, Duwa R, Bhurtel S, et al. Enhancement of blood-brain barrier penetration and the neuroprotective effect of resveratrol. *J Control Release*. 2022;346:1–19. doi:10.1016/j.jconrel.2022.04.003
25. Mi P, Cabral H, Kataoka K. Ligand-Installed Nanocarriers toward Precision Therapy. *Adv Mater*. 2020;32(13):1–29. doi:10.1002/adma.201902604
26. Hoyos-Ceballos GP, Ruozzi B, Ottonelli I, et al. PLGA-PEG-ANG-2 nanoparticles for blood-brain barrier crossing: proof-of-concept study. *Pharmaceutics*. 2020;12(1):210–221. doi:10.3390/pharmaceutics12010072
27. Rauch JN, Luna G, Guzman E, et al. LRP1 is a master regulator of tau uptake and spread. *Nature*. 2020;580(7803):381–385. doi:10.1038/s41586-020-2156-5
28. Shi X, Wang Z, Ren W, et al. LDL receptor-related protein 1 (LRP1), a novel target for opening the blood-labyrinth barrier (BLB). *Signal Transduct Target Ther*. 2022;7(1):175. doi:10.1038/s41392-022-00995-z
29. Kafa H, Wang JT, Rubio N, et al. Translocation of LRP1 targeted carbon nanotubes of different diameters across the blood-brain barrier in vitro and in vivo. *J Control Release*. 2016;225:217–229. doi:10.1016/j.jconrel.2016.01.031
30. Demeule M, Régina A, Ché C, et al. Identification and design of peptides as a new drug delivery system for the brain. *J Pharmacol Exp Ther*. 2008;324(3):1064–1072. doi:10.1124/jpet.107.131318
31. Lillis AP, Mikhailenko I, Strickland DK. Beyond endocytosis: LRP function in cell migration, proliferation and vascular permeability. *J Thromb Haemost*. 2005;3(8):1884–1893. doi:10.1111/j.1538-7836.2005.01371.x
32. Ou Z, Li X, You Y, Liu D, Wang J. Interpreting the therapeutic efficiency of multifunctional hybrid nanostructure against glioblastoma. *ACS Omega*. 2023;8(13):12259–12267. doi:10.1021/acsomega.2c08265

33. Demeule M, Currie JC, Bertrand Y, et al. Involvement of the low-density lipoprotein receptor-related protein in the transcytosis of the brain delivery vector angiopep-2. *J Neurochem*. 2008;106(4):1534–1544. doi:10.1111/j.1471-4159.2008.05492.x
34. Liu C, Liu XN, Wang GL, et al. A dual-mediated liposomal drug delivery system targeting the brain: rational construction, integrity evaluation across the blood-brain barrier, and the transporting mechanism to glioma cells. *Int J Nanomed*. 2017;12:2407–2425. doi:10.2147/ijn.S131367
35. Gao JQ, Lv Q, Li LM, et al. Glioma targeting and blood-brain barrier penetration by dual-targeting doxorubicin liposomes. *Biomaterials*. 2013;34(22):5628–5639. doi:10.1016/j.biomaterials.2013.03.097
36. Jackson-Lewis V, Przedborski S. Protocol for the MPTP mouse model of Parkinson's disease. *Nat Protoc*. 2007;2(1):141–151. doi:10.1038/nprot.2006.342
37. Fishman JB, Rubin JB, Handrahan JV, Connor JR, Fine RE. Receptor-mediated transcytosis of transferrin across the blood-brain barrier. *J Neurosci Res*. 1987;18(2):299–304. doi:10.1002/jnr.490180206
38. Williams SK, Greener DA, Solenski NJ. Endocytosis and exocytosis of protein in capillary endothelium. *J Cell Physiol*. 1984;120(2):157–162. doi:10.1002/jcp.1041200208
39. Sun Y, Yuan K, Mo X, et al. Tyndall-Effect-inspired assay with gold nanoparticles for the colorimetric discrimination and quantification of mercury ions and glutathione. *Talanta*. 2022;238(Pt 1):122999. doi:10.1016/j.talanta.2021.122999
40. Calvo P, Gouritin B, Chacun H, et al. Long-circulating PEGylated polycyanoacrylate nanoparticles as new drug carrier for brain delivery. *Pharm Res*. 2001;18(8):1157–1166. doi:10.1023/a:1010931127745
41. Mura S, Hillaireau H, Nicolas J, et al. Influence of surface charge on the potential toxicity of PLGA nanoparticles towards Calu-3 cells. *Int J Nanomed*. 2011;6:2591–2605. doi:10.2147/ijn.S24552
42. Xiao W, Wang Y, Zhang H, et al. The protein Corona hampers the transcytosis of transferrin-modified nanoparticles through blood-brain barrier and attenuates their targeting ability to brain tumor. *Biomaterials*. 2021;274:120888. doi:10.1016/j.biomaterials.2021.120888
43. Amadio M, Osera C, Lupo G, et al. Protein kinase C activation affects, via the mRNA-binding Hu-antigen R/ELAV protein, vascular endothelial growth factor expression in a pericytic/endothelial coculture model. *Mol Vis*. 2012;18:2153–2164.
44. Chen L, Sutharsan R, Lee JL, et al. Claudin-5 binder enhances focused ultrasound-mediated opening in an in vitro blood-brain barrier model. *Theranostics*. 2022;12(5):1952–1970. doi:10.7150/thno.65539
45. Shih Y, Venault A, Tayo LL, et al. A zwitterionic-shielded carrier with ph-modulated reversible self-assembly for gene transfection. *Langmuir*. 2017;33(8):1914–1926. doi:10.1021/acs.langmuir.6b03685
46. Hao X, Gai W, Wang L, et al. 5-Boronopicolinic acid-functionalized polymeric nanoparticles for targeting drug delivery and enhanced tumor therapy. *Mater Sci Eng C Mater Biol Appl*. 2021;119:111553. doi:10.1016/j.msec.2020.111553
47. Lockman PR, Koziara JM, Mumper RJ, Allen DD. Nanoparticle surface charges alter blood-brain barrier integrity and permeability. *J Drug Target*. 2004;12(9–10):635–641. doi:10.1080/10611860400015936
48. Abbott NJ, Patabendige AA, Dolman DE, Yusof SR, Begley DJ. Structure and function of the blood-brain barrier. *Neurobiol Dis*. 2010;37(1):13–25. doi:10.1016/j.nbd.2009.07.030
49. Kim J, Eygeris Y, Ryals RC, Jozić A, Sahay G. Strategies for non-viral vectors targeting organs beyond the liver. *Nat Nanotechnol*. 2024;19(4):428–447. doi:10.1038/s41565-023-01563-4
50. Blanco E, Shen H, Ferrari M. Principles of nanoparticle design for overcoming biological barriers to drug delivery. *Nat Biotechnol*. 2015;33(9):941–951. doi:10.1038/nbt.3330
51. Cramb KML, Beccano-Kelly D, Cragg SJ, Wade-Martins R. Impaired dopamine release in Parkinson's disease. *Brain*. 2023;146(8):3117–3132. doi:10.1093/brain/awad064
52. Dauer W, Przedborski S. Parkinson's disease: mechanisms and models. *Neuron*. 2003;39(6):889–909. doi:10.1016/s0896-6273(03)00568-3
53. Fearnley JM, Lees AJ. Ageing and Parkinson's disease: substantia nigra regional selectivity. *Brain*. 1991;114(Pt 5):2283–2301. doi:10.1093/brain/114.5.2283
54. Zhang Y, Long H, Zhou F, et al. Echinacoside's nigrostriatal dopaminergic protection against 6-OHDA-Induced endoplasmic reticulum stress through reducing the accumulation of Seipin. *J Cell Mol Med*. 2017;21(12):3761–3775. doi:10.1111/jcmm.13285
55. Zhang T, Wang T, Chen X, Zhao Z, Chen Z. Gut microbiota relieves inflammation in the substantia nigra of chronic Parkinson's disease by protecting the function of dopamine neurons. *Exp Ther Med*. 2022;23(1):52. doi:10.3892/etm.2021.10974
56. Han TY, Yang D, Zhou SQ, et al. Regulative effect of active components of Cistanche deserticola on intestinal dysbacteriosis induced by antibiotics in mice. *Zhongguo Ying Yong Sheng Li Xue Za Zhi*. 2022;38(6):766–770. doi:10.12047/j.cjap.6381.2022.139
57. Subramaniam SR, Chesselet MF. Mitochondrial dysfunction and oxidative stress in Parkinson's disease. *Prog Neurobiol*. 2013;106–107:17–32. doi:10.1016/j.pneurobio.2013.04.004
58. Trist BG, Hare DJ, Double KL. Oxidative stress in the aging substantia nigra and the etiology of Parkinson's disease. *Aging Cell*. 2019;18(6):13031–13054. doi:10.1111/ace.13031
59. Schieber M, Chandel NS. ROS function in redox signaling and oxidative stress. *Curr Biol*. 2014;24(10):453–462. doi:10.1016/j.cub.2014.03.034
60. Goldim MPS, Della Giustina A, Petronilho F. Using evans blue dye to determine blood-brain barrier integrity in rodents. *Curr Protoc Immunol*. 2019;126(1):e83. doi:10.1002/cpim.83

International Journal of Nanomedicine

Dovepress

Publish your work in this journal

The International Journal of Nanomedicine is an international, peer-reviewed journal focusing on the application of nanotechnology in diagnostics, therapeutics, and drug delivery systems throughout the biomedical field. This journal is indexed on PubMed Central, MedLine, CAS, SciSearch®, Current Contents®/Clinical Medicine, Journal Citation Reports/Science Edition, EMBase, Scopus and the Elsevier Bibliographic databases. The manuscript management system is completely online and includes a very quick and fair peer-review system, which is all easy to use. Visit <http://www.dovepress.com/testimonials.php> to read real quotes from published authors.

Submit your manuscript here: <https://www.dovepress.com/international-journal-of-nanomedicine-journal>